

D.V. PODANCHUK, A.A. GOLOBORODKO, M.M. KOTOV, D.A. PETRIV

Taras Shevchenko National University of Kyiv,  
Faculty of Radiophysics, Electronics, and Computer Systems  
(64/13, Volodymyrs'ka Str., Kyiv 01601, Ukraine; e-mail: angol@univ.kiev.ua)

## TALBOT SENSOR WITH DIFFRACTION GRATING ADAPTATION TO WAVEFRONT ABERRATIONS

PACS 42.25.Fx, 42.30.-d

*The results obtained at simulating the functioning of an adaptive sensor based on the Talbot effect are reported. The input grating period was varied depending on the examined wavefront shape and provided the constant observation plane corresponding to the Talbot plane for a plane wave. Using the spherical and astigmatic wavefronts as an example, it is shown that this method can make the sensor measurement range several times wider, by retaining the original angular sensitivity.*

*Keywords:* wavefront, Talbot effect, wavefront sensor.

### 1. Introduction

Optical diagnostics of an inhomogeneous object consists in researching the characteristics of optical radiation passed through it or reflected from its surface [1–3]. Nowadays, a widely used method is the determination of light beam aberrations with the help of wavefront sensors [4]. One of the most promising among them for this purpose is undoubtedly the sensor based on the Talbot effect [5]. The mechanism of its functioning is as follows. If the periodic grating is illuminated with a monochromatic wave with aberrations, its image in the Talbot plane becomes distorted [6, 7]. The input wavefront is reconstructed by comparing this image with the grating image obtained in the Talbot plane for a plane electromagnetic wave (similarly to the reconstruction used in the Shack–Hartmann wavefront sensor) [8]. At the same time, the sensor based on the Talbot effect has a better spatial resolution. In addition, it is simpler in realization [9]. This is so because the binary gratings with a period much shorter than the size of microlenses in the microlens array can be

used. Moreover, they are much simpler for their manufacture.

The basic feature of the Talbot sensor, as well as of the Shack–Hartmann one, is a contradiction between the angular sensitivity and the angular measurement range [10]. For shorter grating periods, the measurement range increases, but the required angular sensitivity is lost. On the contrary, if the grating period grows, the sensor sensitivity also increases, but the measurement range decreases. This problem can be solved by applying holographic microlens arrays in the Shack–Hartmann sensor [11] and holographic gratings in the Talbot one [12]. However, this is rather a laborious procedure. In this work, we consider a possibility of a simpler sensor adaptation to the changes in the examined wavefront.

### 2. Basic Relations

The diffraction pattern in the Talbot plane is calculated using an approximation given by the Huygens–Fresnel principle [4]. Let a plane wave  $U_0$  normally fall on a two-dimensional periodic structure with the complex amplitude transmittance

$$T(x, y) = \sum_{n,m=-\infty}^{\infty} A_n A_m e^{i \frac{2\pi}{\Delta} (nx + my)}, \quad (1)$$

*ISSN 2071-0194. Ukr. J. Phys. 2015. Vol. 60, No. 1*

where  $\Delta$  is the structure period, and  $A_n$  and  $A_m$  are the expansion coefficients. Then the image obtained in the Talbot plane

$$Z_T = 2\Delta^2/\lambda, \quad (2)$$

where  $\lambda$  is the wavelength, reproduces the periodic structure (1):

$$U(x, y|Z_T) = U_0 e^{-i\frac{2\pi}{\lambda}Z_T} \times \\ \times \sum_{n,m=-\infty}^{\infty} A_n A_m e^{i2\pi \frac{n(x+\Delta)+m(y+\Delta)}{\Delta}}, \quad (3)$$

which is equivalent to

$$U(x, y|Z_T) = U_0 e^{-i\frac{2\pi}{\lambda}Z_T} T(x, y). \quad (4)$$

This self-reproduction of a grating is called the Talbot effect [13]. If the grating is illuminated by a wave with the characteristic orthogonal radii of the wavefront curvature  $R_X$  and  $R_Y$ , the incident light wave amplitude can be expressed in the form [14]

$$U_D(x, y|0) = U_0 e^{i\frac{\pi x^2}{\lambda R_X}} e^{i\frac{\pi y^2}{\lambda R_Y}}. \quad (5)$$

The field distribution in the Talbot plane is changed in the following way:

$$U(x, y|Z_T) = U_D(x, y|0) e^{-i\frac{2\pi}{\lambda}Z_T} \times \\ \times \sum_{n=-\infty}^{\infty} A_n e^{i\frac{\pi R_X n}{Z_T + R_X} \left( \frac{2x}{\Delta} - \frac{\lambda Z_T n}{d^2} \right)} \times \\ \times \sum_{m=-\infty}^{\infty} A_m e^{i\frac{\pi R_Y m}{Z_T + R_Y} \left( \frac{2y}{\Delta} - \frac{\lambda Z_T m}{d^2} \right)}. \quad (6)$$

Here,  $d$  is the size of the transparent part. In this case, the argument of the exponential function in Eq. (6) becomes a multiple of  $2\pi$  only in the planes

$$Z_{X,Y} = \frac{Z_T}{1 - \frac{Z_T}{R_{X,Y}}}, \quad (7)$$

and the image in the Talbot plane is blurred. Therefore, in the case where the wavefront curvatures are different in the orthogonal directions, there is no unique grating period that would restore the sharpness plane position. This means that, in order to obtain a partially self-reproduced image, the photodetector has

to be shifted into the plane  $Z_X$  or  $Z_Y$ , which would require a lot of time.

It is worth noting that expression (6) is applicable only in the small-angle approximation,  $d \gg n\lambda$ . Therefore, for the effect to be observed, it is necessary that the spatial spectrum of grating (1) should not contain large  $A_n$  with  $n > 0.1d/\lambda$  [7]. In this case, as was shown in work [15], the transverse displacement of aperture images is determined by the average local inclination within the nearest 3–4 grating apertures, whereas aberrations of the second order are responsible for a variation of the image shape.

The idea of Talbot sensor adaptation is as follows. Leaving a photodetector in the plane  $Z_T$ , we should change the period of the input grating depending on the curvature of the analyzed wavefront. It is necessary that the observation plane should be an effective Talbot plane for the incident wavefront. Then, for a spherical wave with radius  $R$ , the period is determined by the relation

$$\Delta_R = \sqrt{\frac{Z_T R \lambda}{2(Z_T + R)}}. \quad (8)$$

For the astigmatic wave, which is characterized by two curvature radii,  $R_X$  and  $R_Y$ , the grating should have different periods along the corresponding axes:

$$\Delta_{X,Y} = \sqrt{\frac{Z_T R_{X,Y} \lambda}{2(Z_T + R_{X,Y})}}. \quad (9)$$

Now, it is evident that the grating periods along the axes  $x$  and  $y$  do not coincide. In this case, the illumination of such a grating with an astigmatic wave restores the periodic structure in the Talbot plane. Therefore, in view of the aforesaid, we may say about the Talbot effect for a “deformed” grating.

We used an iterative method in order to extend the measurement range [16]. The method consists in that we select the wavefront with a curvature lying beyond the range taken in the zeroth iteration as the reference one; we also take a new grating with such a period that the effective Talbot distance for the new basic wavefront should be equal to the distance from the grating to the observation plane in the previous iteration. The curvature of the measured wavefront is calculated by summing up the result obtained for the restored wavefront and the curvature of the reference wavefront. The measurement ranges of next

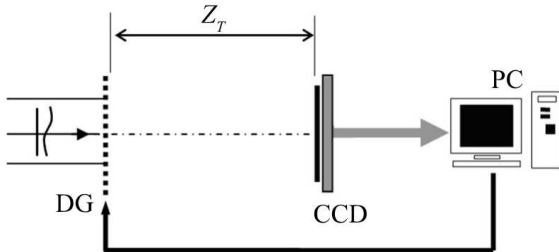


**Fig. 1.** Schematic diagram of an adaptive Talbot sensor used at the simulation

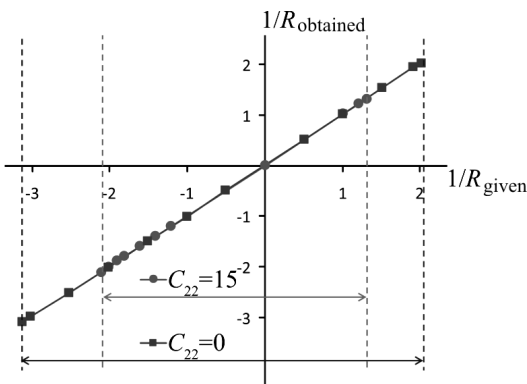


**Fig. 2.** Evaluation of curvature measurement ranges for the waves without astigmatism ( $C_{22} = 0$ ) and with constant astigmatism ( $C_{22} = 15$ )

iterations are overlapped so that, within the overlapping interval, it is possible to restore aberrations with the highest possible accuracy in one of the iterations. Hence, the Talbot sensor can be adapted to the magnitude of wavefront curvature without changing the observation plane.

### 3. Results and Their Discussion

Some capabilities of an adaptive Talbot sensor were studied by simulating the corresponding experiment in accordance with the formulas of the amplitude distribution in the Talbot plane, Eqs. (4) and (6). The simulated experimental setup is shown in Fig. 1. The examined wavefront falls on a diffraction grating (DG). The image is registered by a photodetector (CCD) located at the Talbot distance. Depending on the curvature of the incident wavefront, the computer (PC) changes the grating period.

The simulation consisted of the following consecutive stages: wavefront initialization; calculation of the illuminance in the image plane at the Talbot dis-

tance; determination of local displacements of image points, wavefront reconstruction; and comparison of the restored and input wavefronts. The measurement ranges for a spherical wavefront with and without astigmatism were analyzed. A  $25 \times 25$ -grating was taken for calculations. The wavefront aberrations were modeled by the corresponding Zernike polynomials [17]

$$Z_{20}(x, y) = \frac{x^2 + y^2}{r^2}, \quad (10)$$

$$Z_{22}(x, y) = \frac{x^2 - y^2}{r^2}, \quad (11)$$

where  $r = 2$  mm is the radius of the sensor aperture. The aberration coefficients are given in terms of the radius  $R_{20}$ , which corresponds to the radius for defocusing ( $R = R_{20}$  in Eq. (8)), and the radius  $R_{22}$ , which corresponds to the radii for astigmatism ( $R_X = -R_Y = R_{22}$  in Eq. (9)). Hence, the aberration coefficients of defocusing,

$$C_{20} = \frac{\pi r^2}{2\lambda R_{20}}, \quad (12)$$

and astigmatism,

$$C_{22} = \frac{\pi r^2}{\lambda R_{22}}, \quad (13)$$

are determined in terms of the characteristic radii of the wavefront curvature, spherical  $R_{20}$  and astigmatic  $R_{22}$ .

The results of simulation measurements are presented in Fig. 2. One can see that, without astigmatism, the sensor works in the range from  $C_{20} = -31$  ( $1/R = -3.12 \text{ m}^{-1}$ ) to  $C_{20} = 20$  ( $1/R = 2.02 \text{ m}^{-1}$ ) and, for a wave with astigmatism ( $C_{22} = 15$ ), from  $C_{20} = -21$  ( $1/R = -2.11 \text{ m}^{-1}$ ) to  $C_{20} = 13$  ( $1/R = 1.31 \text{ m}^{-1}$ ). It is worth noting that, in the absence of astigmatism, the Talbot sensor has a wider measurement range.

In Fig. 3, the fragments of grating images calculated at the range limits (panels *a* and *d*) and beyond them (panels *b* and *e*) are depicted. The images in panels *b* and *e* are so distorted that the wavefront cannot be measured. In order to measure it without changing the position of the observation plane, we changed the grating period in such a manner that the observation plane became the effective Talbot plane for the wavefronts with aberrations corresponding to

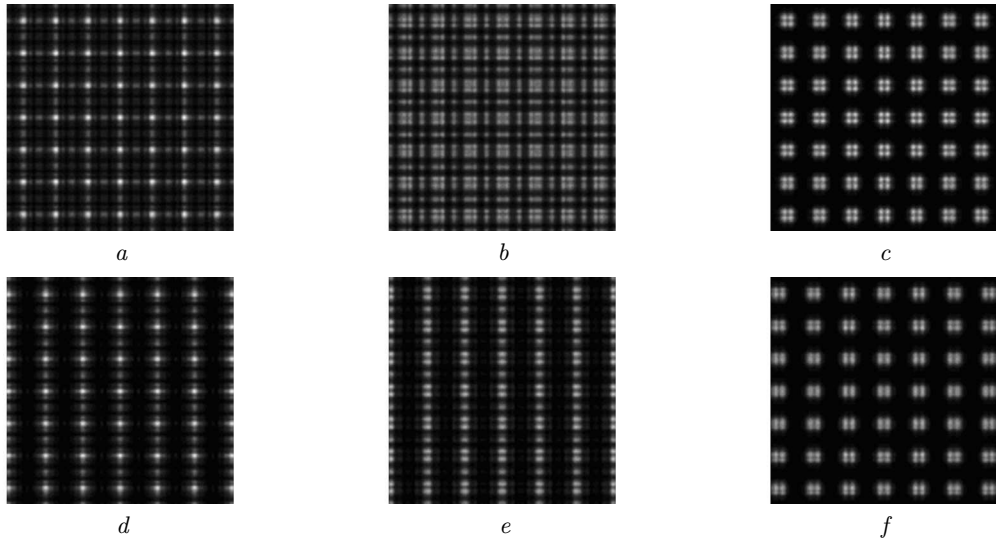


**Fig. 3.** Fragments of images obtained in the Talbot observation plane when illuminating gratings with various periods, by using waves with aberrations: *a* –  $\Delta = 160 \mu\text{m}$ ,  $C_{20} = 20$ ,  $C_{22} = 0$ ; *b* –  $\Delta = 160 \mu\text{m}$ ,  $C_{20} = 22$ ,  $C_{22} = 0$ ; *c* –  $\Delta = 174.88 \mu\text{m}$ ,  $C_{20} = 22$ ,  $C_{22} = 0$ ; *d* –  $\Delta = 160 \mu\text{m}$ ,  $C_{20} = 13$ ,  $C_{22} = 15$ ; *e* –  $\Delta = 160 \mu\text{m}$ ,  $C_{20} = 15$ ,  $C_{22} = 15$ ; *f* –  $\Delta_X = 163.71 \mu\text{m}$ ,  $\Delta_Y = 17.31 \mu\text{m}$ ,  $C_{20} = 15$ ,  $C_{22} = 15$

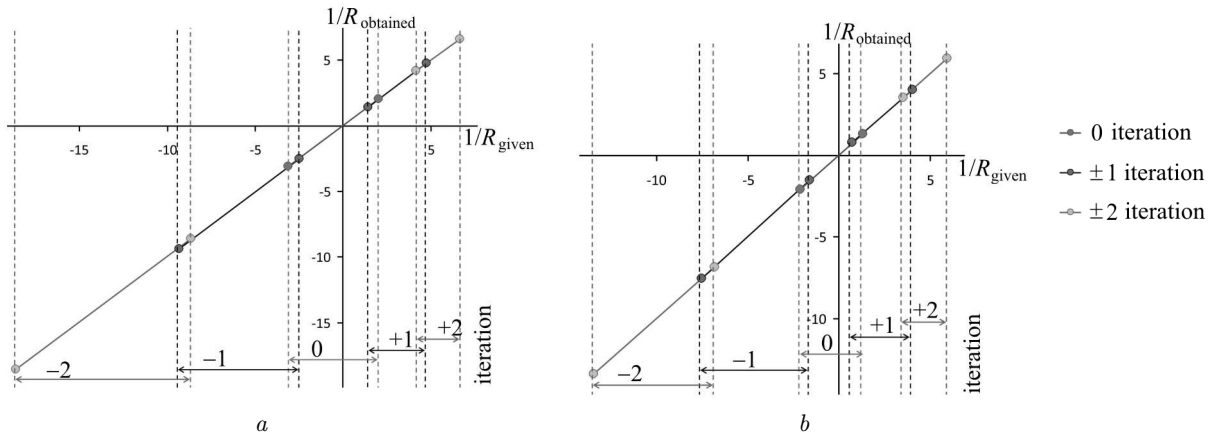


**Fig. 4.** Ranges of curvature measurements using the adaptive Talbot sensor for the spherical ( $C_{22} = 0$ ) (a) and astigmatic ( $C_{22} = 15$ ) (b) wavefronts

#### Iterative algorithm for measuring the optical wavefront with aberrations

| Iteration | $C_{22} = 0$ |                      |                       |                                  |                                  | $C_{22} = 15$ |                      |                         |                         |                                  |                                  |
|-----------|--------------|----------------------|-----------------------|----------------------------------|----------------------------------|---------------|----------------------|-------------------------|-------------------------|----------------------------------|----------------------------------|
|           | $C_{20}$     | $1/R, \text{m}^{-1}$ | $\Delta, \mu\text{m}$ | $1/R \text{ min}, \text{m}^{-1}$ | $1/R \text{ max}, \text{m}^{-1}$ | $C_{20}$      | $1/R, \text{m}^{-1}$ | $\Delta_X, \mu\text{m}$ | $\Delta_Y, \mu\text{m}$ | $1/R \text{ min}, \text{m}^{-1}$ | $1/R \text{ max}, \text{m}^{-1}$ |
| 0         | 0            |                      | 160                   | -3.09                            | 2.01                             | 0             |                      | 160                     | 160                     | -2.12                            | 1.30                             |
| +1        | 30           | 3.02                 | 183.12                | 1.41                             | 4.75                             | 25            | 2.52                 | 172.79                  | 186.61                  | 0.77                             | 4.02                             |
| -1        | -50          | -5.04                | 134.49                | -9.39                            | -2.53                            | -40           | -4.03                | 136.46                  | 142.97                  | -7.55                            | -1.56                            |
| +2        | 50           | 5.04                 | 206.49                | 4.18                             | 6.61                             | 50            | 5.04                 | 199.8                   | 222.08                  | 3.54                             | 5.93                             |
| -2        | -110         | -11.08               | 115.95                | -18.6                            | -8.63                            | -100          | -10.08               | 116.82                  | 120.82                  | -13.42                           | -6.87                            |

the range limits. Now, if those wavefronts are taken as the reference ones, the measurement range shifts, and we can restore the wavefront located outside the previous range.

In the following simulation experiment, the iterative method was applied in order to expand the measurement ranges shown in Fig. 2. The reference wavefront and the grating period in every iteration were selected to provide the overlapping of the measurement ranges of consecutive iterations. The parameters of the adaptive sensor for every iteration are listed in Table, and the corresponding measurement ranges are shown in Fig. 4.

The total measurement range obtained for the sensor without astigmatism extends from  $C_{20} = -185$  ( $1/R = -18.6 \text{ m}^{-1}$ ) to  $C_{20} = 66$  ( $1/R = 6.61 \text{ m}^{-1}$ ), and with astigmatism ( $C_{22} = 15$ ) from  $C_{20} = -120$  ( $1/R = -13.42 \text{ m}^{-1}$ ) to  $C_{20} = 58$  ( $1/R = -5.93 \text{ m}^{-1}$ ). Hence, the dynamic range of the adaptive sensor based on the Talbot effect was increased by a factor of 5 in the case of the optical wave without astigmatism and by a factor of 5.6 in the case of the optical wave with astigmatism ( $C_{22} = 15$ ).

#### 4. Conclusions

A new method of measurement of wavefront aberrations is proposed and demonstrated for the first time. It is based on the observation of the Talbot effect when the diffraction grating is adapted to the wavefront curvature of the analyzed wave. It is shown that, with the help of the adaptive Talbot sensor, the measurement range can be made several times wider, by retaining the required angular sensitivity. A possibility of the self-reproduction of the deformed (with different period ratios along the axes) grating by the astigmatic wavefront is demonstrated. The advantages of the proposed method at the application to the solution of adaptive optics problems with the use of diffraction gratings based on dynamic spatial light modulators should be emphasized.

*The authors express their sincere gratitude to Academician of the NAS of Ukraine M.G. Nakhodkin who was the initiator of a series of researches dealing with the properties of fields scattered by structured and stochastic media.*

- O. Azucena, J. Crest, S. Kotadia, W. Sullivan, X. Tao, M. Reinig, D. Gavel, S. Olivier, and J. Kubby, Opt. Lett. **36**, 825 (2011).

- A.A. Goloborodko, V.N. Kurashov, D.V. Podanchuk, and N. S. Sutyagina, Proc. SPIE **7008**, 70081S (2008).
- S. Manzanera, C. Canovas, P.M. Prieto, and P. Artal, Opt. Expr. **16**, 7748 (2008).
- G. Rousset, in *Adaptive Optics for Astronomy*, edited by D.M. Alloin and J.-M. Mariotti (Kluwer, Dordrecht, 1994), p. 116.
- A. Koryakovskiy and V. Marchenko, Techn. Phys. **51**, 1432 (1981).
- R. Sekine, T. Shibuya, K. Ukai, S. Komatsu, M. Hattori, T. Mihashi, N. Nakazawa, and Y. Hirihara, Opt. Rev. **13**, 207 (2006).
- D. Podanchuk, A. Kovalenko, V. Kurashov, M. Kotov, A. Goloborodko, and V. Danko, Appl. Opt. **53**, B223 (2014).
- S. Thomas, T. Fusco, A. Tokovinin, M. Nicolle, V. Michau, and G. Rousset, Mon. Not. R. Astron. Soc. **371**, 323 (2006).
- D.V. Podanchuk, V.N. Kurashov, A.A. Goloborodko, V. P. Dan'ko, M. M. Kotov, and O. O. Parhomenko, Proc. SPIE **8338**, 83380G (2011).
- A. Goloborodko, V. Grygoruk, M. Kotov, V. Kurashov, D. Podanchuk, and N. Sutyagina, Ukr. J. Phys. **53**, 946 (2008).
- J.-Y. Son, D. Podanchuk, V. Dan'ko, and K.-D. Kwak, Opt. Eng. **42**, 3389 (2003).
- D. Podanchuk, V. Kurashov, A. Goloborodko, V. Dan'ko, M. Kotov, and N. Goloborodko, Appl. Opt. **51**, C125 (2012).
- P. Latimer and R.F. Crouse, Appl. Opt. **31**, 80 (1992).
- J.W. Goodman, *Introduction to Fourier Optics* (McGraw-Hill, New York, 1996).
- A. Kovalenko, M. Kotov, V. Kurashov, and M. Movchan, Proc. SPIE **9066**, 90660R (2013).
- D.V. Podanchuk, V.P. Dan'ko, A.A. Goloborodko, and N.S. Sutyagina, Proc. SPIE **7388**, 73880Q (2009).
- L. Lundström and P. Unsbo, J. Opt. Soc. Am. A **24**, 569 (2007).

Received 23.10.14.

Translated from Ukrainian by O.I. Voitenko

Д.В. Поданчук, А.О. Голобородько,

М.М. Котов, Д.А. Петрів

СЕНСОР ТАЛБОТА ІЗ АДАПТАЦІЄЮ  
ДИФРАКЦІЙНОЇ ГРАТКИ ДО АБЕРАЦІЙ  
ДОСЛІДЖУВАНОГО ХВИЛЬОВОГО ФРОНТУ

Р е з ю м е

В роботі приведено результати моделювання роботи адаптивного сенсора на основі ефекту Талбота. У моделі змінювався період вхідної гратки залежно від аберрацій досліджуваного хвильового фронту при незмінній площині спостереження, яка відповідає площині Талбота для плоскої хвилі. На прикладі сферичного та астигматичного хвильового фронтів показано, що за допомогою такого методу можна в декілька разів розширити діапазон вимірювань сенсора, зберігаючи при цьому необхідну кутову чутливість.